A multilaminate soil model for highly overconsolidated clays

Un modèle de sol multi-plan pour les argiles fortement surconsolidées

B. Schädlich & H. F. Schweiger
Institute for Soil Mechanics and Foundation Engineering, Graz University of Technology, Austria

ABSTRACT

This paper presents a novel approach to model the shear strength of highly overconsolidated, stiff clays in numerical analysis. The multilaminate framework of the model is explained, and details of the yield surfaces, plastic potential functions and hardening rules are given. Comparison of undrained stress paths predicted by the model and laboratory test results shows that the model is well suited to predict peak strength and dilatant behavior typical for overconsolidated soils.

RÉSUMÉ

Cet article présente une approche originale pour modéliser numériquement la résistance au cisaillement des argiles raides fortement surconsolidés. Le modèle multi-plan est expliqué et les surfaces seuils de plasticité, les potentiels plastiques et les lois d'écrouissage sont détaillés. La comparaison des chemins de contrainte non-drainés prédits par le modèle d'une part et résultants d'un essai de laboratoire d'autre part, montre que le modèle est bien adapté à la prédiction du pic de résistance et du comportement dilatant typique des sols surconsolidés.

Keywords: Hvorslev surface, overconsolidated clay, multilaminate soil models

1 INTRODUCTION

The behavior of highly overconsolidated, stiff clays differs substantially from normally consolidated soils: Overconsolidated clays are characterized by lower void ratio, higher shear strength and usually anisotropic material parameters. In natural, undisturbed samples shear strength can be further increased by inter-particle bonding and cementation, resulting in gradual transition to soft rock materials. After reaching peak strength, strain localization occurs and shear strength reduces with increasing plastic deformation (strain softening). Although noted very early in experimental testing, taking all these aspects into account in constitutive modeling proved to be rather difficult. Furthermore, performing strain softening analysis with conventional Finite Element programs causes additional problems due to severe mesh dependency, if no appropriate regularization technique is employed. As a result, the number of constitutive soil models accounting for all these characteristics is limited, and application to practical boundary value problems is still rare.

In this study an extension of existing multilaminate soil models [5] is presented, which accounts for peak strength and its dependency on volume change by utilizing the concept of a Hvorslev-type strength surface. Model predictions are compared with experimental data on Vallericca clay.

2 SHEAR STRENGTH OF HIGHLY OVERCONSOLIDATED CLAYS

With respect to the pioneering work of Hvorslev the envelope of shear strength on the highly overconsolidated side of the critical state line is commonly termed Hvorslev surface. On a line of constant volume in the V-p-q space (which is equivalent to an undrained stress path) the Hvorslev surface can be plotted as a straight line with a cohesion intercept at p' = 0 and inclination m_{HV}.

At the intersection with the critical state line the Hvorslev surface is connected to the Roscoe – Rendulic surface. The cohesion intercept is no material constant but depends on the current void ratio e. As the soil volume differs along the unloading/reloading line, also q_{HV} changes with varying level of overconsolidation. By normalizing the shear strength q_{max} to the equivalent pressure p_e on the isotropic compression line (ICL), dependency on soil volume can be extracted and a unique contour of shear strength is obtained (Figure 1).

$$\frac{q_{\max}}{p'_e} = m_{HV} \cdot \frac{p'}{p'_e} + q_{HV} \tag{1}$$

The projection of the shear strength envelope above an unloading reloading line in the p-q-space plots as a curved line, touching the critical state line at the origin of axis and at the intersection with the Roscoe-Rendulic surface.

It is worth noting that also for rock materials the concept of a Hvorslev envelope has been found suitable to some extent to describe the strength and deformation behavior [4].

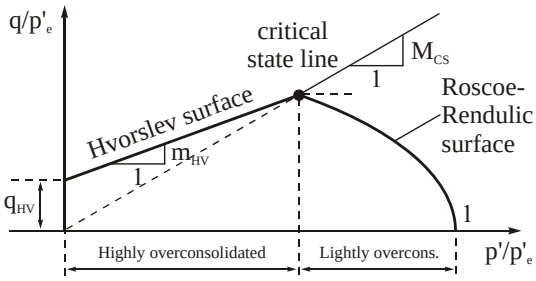

Figure 1: Normalized shear strength contours

3 BASIC MULTILAMINATE MODEL

Multilaminate constitutive models are based on the concept that the material behavior can be formulated on a distinct number of local planes with varying orientation. Each plane represents a sector of a virtual sphere of unit radius around the stress point and is assigned a weight factor according to the proportion of its sector with regard to the volume of the unit sphere. The global response of the material to a prescribed load is obtained by summation of the contributions of all planes.

Within the multilaminate concept the local stresses are assumed to be a projection of the global stress state (static constraint). Conceptually similar models based on the kinematic constraint (local strain increments are a projection of the global strain increment) are the so-called microplane models.

The multilaminate constitutive model presented in this study is an extension of existing elastoplastic models of this type [5]. In the following the stress point algorithm for initially isotropic material is briefly explained.

The macroscopic trial stress $\sigma_{gl,trial}$ is calculated from the global elastic compliance matrix C_{gl} and the global strain increment $d\varepsilon_{gl}$, which is assumed to be elastic in the first iteration. C_{gl} is derived as the weighted sum of the local compliances C_{loc}. In the case of isotropic linear elastic material, C_{loc} is equal for all planes.

$$\boldsymbol{\sigma}_{gl,trial} = \mathbf{C}_{gl} \cdot d\boldsymbol{\varepsilon}_{gl} + \boldsymbol{\sigma}_{gl,old} \tag{2}$$

$$\mathbf{C}_{gl} = 3 \cdot \sum_i \left(\mathbf{T}_i \cdot \mathbf{C}_{i,loc} \cdot \mathbf{T}_i^T \cdot w_i \right) \tag{3}$$

$$\mathbf{C}_{loc} = \begin{pmatrix} Cnn & 0 & 0 \\ 0 & Ctt & 0 \\ 0 & 0 & Ctt \end{pmatrix} \tag{4}$$

$$Cnn = \frac{1-2\nu}{E};\ Ctt = \frac{1+3\nu}{E} \tag{5}$$

The factor of 3 in front of the summation can be derived from the principle of virtual work by comparing the sum of local work contributions and the macroscopic work. The weight factors w_i depend on the chosen integration rule. In this study an integration rule based on 2 × 33 planes [1] is used, which proved to balance well between accuracy and computational cost.

The transformation matrix T_i contains the derivatives of the local stress components with respect to the global stress state. Using a fixed set of local coordinates represented by the unit vector $n_i^T = (n_{i,1}, n_{i,2}, n_{i,3})$ normal to the plane i and two unit tangential vectors within the plane, $s_i^T = (s_{i,1}, s_{i,2}, s_{i,3})$ and $t_i^T = (t_{i,1}, t_{i,2}, t_{i,3})$, these derivates take on constant scalar values.

$$\mathbf{T}_i = \frac{\partial \boldsymbol{\sigma}_{i,loc}}{\partial \boldsymbol{\sigma}_{gl}} = \begin{pmatrix} n_{i,1}^2 & n_{i,1}\cdot s_{i,1} & n_{i,1}\cdot t_{i,1} \\ n_{i,2}^2 & n_{i,2}\cdot s_{i,2} & n_{i,2}\cdot t_{i,2} \\ n_{i,3}^2 & n_{i,3}\cdot s_{i,3} & n_{i,3}\cdot t_{i,3} \\ 2n_{i,1}\cdot n_{i,2} & n_{i,1}\cdot s_{i,2}+n_{i,2}\cdot s_{i,1} & n_{i,1}\cdot t_{i,2}+n_{i,2}\cdot t_{i,1} \\ 2n_{i,2}\cdot n_{i,3} & n_{i,3}\cdot s_{i,2}+n_{i,2}\cdot s_{i,3} & n_{i,3}\cdot t_{i,2}+n_{i,2}\cdot t_{i,3} \\ n_{i,1}\cdot n_{i,3} & n_{i,3}\cdot s_{i,1}+n_{i,1}\cdot s_{i,3} & n_{i,3}\cdot t_{i,1}+n_{i,1}\cdot t_{i,3} \end{pmatrix} \quad (6)$$

By projecting the global trial stress vector $\sigma_{gl,trial}$ with the transformation matrix T_i on plane i, the local trial stress vectors $\sigma_{i,loc}$ are obtained for all planes.

$$\boldsymbol{\sigma}_{i,loc} = \begin{pmatrix} \sigma_{n,i} \\ \tau_{s,i} \\ \tau_{t,i} \end{pmatrix} = \left(\mathbf{T}_i\right)^T \cdot \boldsymbol{\sigma}_{gl,trial} \quad (7)$$

Plastic strains are calculated locally based on strain hardening elastoplasticity. Back-transformation and summation of all local plastic strains delivers the global plastic strain increment.

$$d\boldsymbol{\varepsilon}_{i,loc}^{pl} = \lambda_i \cdot \frac{\partial g_i}{\partial \boldsymbol{\sigma}_{i,loc}} \quad (8)$$

$$\lambda_i = \frac{f^{trial}}{\frac{\partial f_i}{\partial \boldsymbol{\sigma}_{i,loc}} \cdot \mathbf{C}_{i,loc}^{-1} \cdot \frac{\partial g_i}{\partial \boldsymbol{\sigma}_{i,loc}} - \frac{\partial f_i}{\partial \boldsymbol{\varepsilon}_{i,loc}^{pl}} \cdot \frac{\partial g_i}{\partial \boldsymbol{\sigma}_{i,loc}}} \quad (9)$$

$$d\boldsymbol{\varepsilon}_{gl}^{pl} = 3 \cdot \sum_i \mathbf{T}_i \cdot d\boldsymbol{\varepsilon}_{i,loc}^{pl} \cdot w_i \quad (10)$$

The new global trial stress is then calculated with the difference of the total strain increment and the plastic strain increment.

$$\boldsymbol{\sigma}_{gl,trial} = \mathbf{C}_{gl} \cdot \left(d\boldsymbol{\varepsilon}_{gl} - d\boldsymbol{\varepsilon}_{gl}^{pl}\right) + \boldsymbol{\sigma}_{gl,old} \quad (11)$$

This iterative procedure is repeated until the plastic strain increment of the current iteration is less than 1% of the total plastic strains calculated in that step.

4 HVORSLEV SURFACE MODEL

4.1 Yield functions and hardening rules

The yield surfaces are defined on plane level in local tangential (shear) stresses τ and normal stresses σ_n. Plastic strains and mobilization of the yield surfaces are allowed to differ from plane to plane, resulting in strain induced anisotropy during plastic loading.

In the model three yield surfaces are defined. The elliptical, strain hardening cap yield surface controls compression behavior in the normally and lightly overconsolidated range.

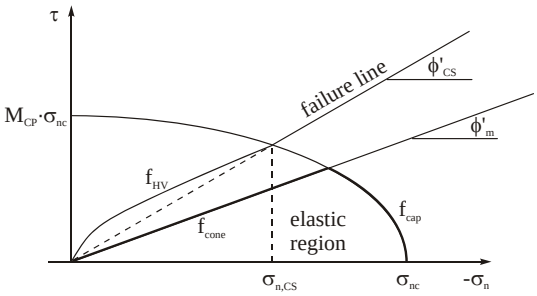

Figure 2: Local yield surfaces

$$f_{cap} = \frac{\sigma_n^2}{\sigma_{nc}^2} + \frac{\tau^2}{\left(M_{CP} \cdot \sigma_{nc}\right)^2} - 1 \qquad (12)$$

The position of the cap yield surface is defined by the intersection with the σ_n –axis and the cap shape parameter MCP, which controls the intersection with the τ-axis. The value of MCP is determined beforehand in an iterative procedure such that in normally consolidated, oedometric conditions $\sigma_h = K_0 \cdot \sigma_v$ is ensured. The initial size of the cap yield surface is defined by the initial stresses and the degree of overconsolidation OCR. For OCR = 1, the cap yield surface is positioned at the initial stress state. If plastic normal strains occur locally, increase or reduction of the cap yield surface is controlled by the corresponding hardening rule (eq. 13). The hardening parameter K contains the volumetric stiffness in primary loading E_{oed} and the elastic unloading/reloading Young's modulus E_{ur}, both at reference pressure p_{ref}. Dependency of stiffness on stress level is taken into account by an exponential law using the power index m (shown for E_{oed} in eq. 15).

$$\sigma_{nc,i+1} = -\left[\left|\sigma_{nc,i}\right|^{1-m} + K \cdot \frac{(m-1)}{p_{ref}^{m-1}} \cdot \Delta\varepsilon_n^{pl} \right]^{\frac{1}{1-m}} \qquad (13)$$

$$K = \frac{3}{p_{ref} \cdot \left[\frac{1}{E_{oed}^{ref}} + \frac{3 \cdot (1-2\nu)}{E_{ur}^{ref}} \right]} \qquad (14)$$

$$E_{oed}^{ref} = E_{oed}^{ref} \cdot \left(\frac{p'}{p_{ref}} \right)^m \qquad (15)$$

The cone yield surface is defined by a straight line and governs plastic deformation in deviatoric loading below the Hvorslev surface. In the normally and slightly overconsolidated range the cone yield surface finally equals the Mohr-Coulomb failure line for $\phi_m = \phi_{CS}$.

$$f_{cone} = \tau + \sigma_n \cdot \tan\varphi_m \qquad (16)$$

The hardening rule (eq. 17) controlling mobilization of the cone yield surface contains the hardening parameter A_{mat}, which defines the local shear strain at which the maximum friction angle ϕ_{max} is mobilized. The maximum friction angle ϕ_{max} depends on the position of the Hvorslev yield surface at the current stress (Figure 5).

$$\tan\varphi_{m,i+1} = \tan\varphi_{m,i} + \frac{\Delta\gamma^{pl} \cdot \left(\tan\varphi_{\max} - \tan\varphi_{m,i}\right)}{\Delta\gamma^{pl} + \frac{A_{mat}}{3} \cdot \frac{\left(\tan\varphi_{\max} - \tan\varphi_0\right)}{\left(\tan\varphi_{\max} - \tan\varphi_{m,i}\right)}} \qquad (17)$$

The strain hardening cone yield surface is active in deviatoric loading until the stress path reaches the Hvorslev strength surface. The principle definition of the Hvorslev surface (eq. 1) is adapted to the multilaminate definition of local stresses by substituting q with τ and p with σ_n. The equivalent normal stress $\sigma_{n,ve}$ at the isotropic compression line is calculated from the current normal stress σ_n and the pre-consolidation stress σ_{nc}.

$$f_{HV} = \tau + \sigma_n \cdot \tan\varphi_e - c_{HV} \qquad (18)$$

$$c_{HV} = B \cdot \left(\frac{\tan\varphi_e}{\tan\varphi_{CS}} - 1 \right) \cdot \sigma_{n,ve} \qquad (19)$$

$$\sigma_{n,ve} = -\left[\left|\sigma_{nc}\right|^{1-m} + \frac{E_{oed}^{ref}}{E_{ur}^{ref}} \cdot \ldots \ldots 3(1-2\nu) \cdot \left(\sigma_n^{1-m} - \sigma_{nc}^{1-m}\right) \right]^{1/(1-m)} \qquad (20)$$

For updating the local pre-consolidation stress σ_{nc} all normal plastic strain contribution of the current plane are taken into account. Positive plastic normal strains, caused by dilatancy at the cone or the Hvorslev yield surface, reduce σ_{nc}, whereas negative plastic normal strains enlarge σ_{nc}.

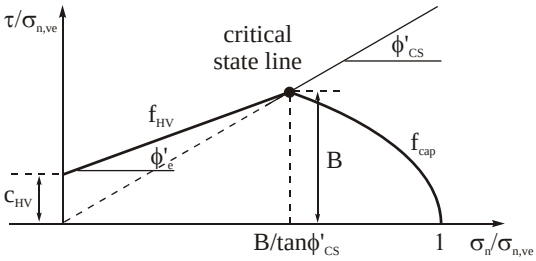

Figure 3: Normalized local shear strength contours

In undrained conditions volumetric plastic strains are compensated on global level by elastic volumetric strains of equal magnitude, such that the volume remains constant ($\varepsilon_{vol} = 0$) and therefore p' changes. In that case $\sigma_{n,ve}$ remains constant, although σ_{nc} gradually decreases throughout the test. In drained conditions strain softening is triggered by the increase in volume und the subsequent reduction of $\sigma_{n,ve}$, which results in decreasing c_{HV} and hence in lower shear strength.

4.2 Plastic potential functions

Plasticity resulting from the cap yield surface is fully associated, which means that the plastic potential function is the same as the cap yield function. Cone and Hvorslev yield surface are non-associated. The cone plastic potential function equals the cone yield function with the friction angle ϕ_m being replaced by the mobilized angle of dilatancy ψ_m (eq. 21). Mobilization of dilatancy is modeled by a cubical function in dependency on the mobilized friction angle ϕ_m (Schweiger et al. 2009, Figure 4).

$$g_{cone} = g_{HV} = \tau + \sigma_n \cdot \tan\psi_m \tag{21}$$

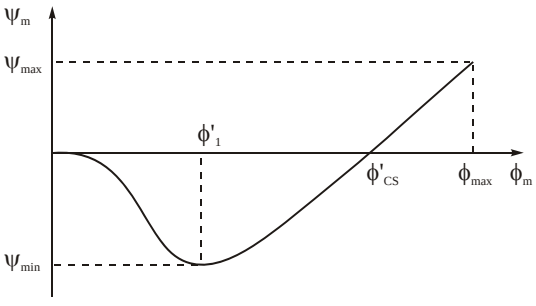

Figure 4: Mobilization of dilatancy

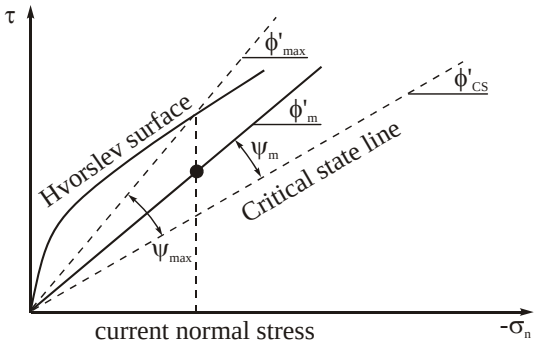

Figure 5: Mobilized and maximum angle of dilatancy

The maximum angle of dilatancy ψ_{max} is calculated from the difference between the critical state line and the Hvorslev surface at to the current local stress state (Figure 5, eq. 22). With that approach a smooth transition from dilatant behavior in the heavily overconsolidated to non-dilatant behavior in the normally consolidated range is achieved. With increasing stress level and accumulating plastic strains ψ_{max} reduces, eventually resulting in $\phi_m = \phi_{CS}$ and $\psi_{max} = \psi_m = 0$ at critical state.

$$\psi_{\max} = \varphi_{\max} - \varphi_{CS} \tag{22}$$

5 COMPARISON WITH EXPERIMENTAL DATA

Burland et al. [2] conducted an extensive research program on the strength properties of four overconsolidated clays, on both intact (natural) and reconstituted samples. The comparison further on focuses on triaxial test results on reconstituted samples of normally and overconsolidated Vallericca clay.

The overconsolidated samples were compressed to an isotropic pre-consolidation pressure of 2000kPa and then swelled isotropically to initial stresses of p'_0 = 100, 200 and 400kPa. The intrinsic stiffness parameters λ and κ (Table 1) are converted to $E_{oed,ref} = p_{ref} \cdot (1+e)/\lambda = 1090$kPa and $E_{ur,ref} = 3p_{ref} \cdot (1-2\nu) \cdot (1+e)/\kappa = 10140$kPa corresponding to the void ratio at the pre-consolidation pressure of 2000kPa.

Table 1. Intrinsic material parameters of Vallericca clay (after [2] and [3])

ϕ_{CS}	ϕ_e	λ	κ	e_{1kPa}
26.7°	22.6°	0.145	0.028	1.68

Experimental and calculated undrained stress paths for the normally and overconsolidated samples are compared in Figure 6. The model predicts the dilatant/compressive behavior of the overconsolidated and normally consolidated samples with good accuracy. If normalized by the equivalent pressure p_e, both experimental and calculated overconsolidated stress paths do not reach the critical state line (Figure 7). In the experiment such behavior can be attributed to the formation of shear bands, triggering local increase in volume and subsequent loss of shear strength. Similarly, in the calculations planes at the most critical orientation preferably develop plastic normal strains, resulting in reduced strength on these planes.

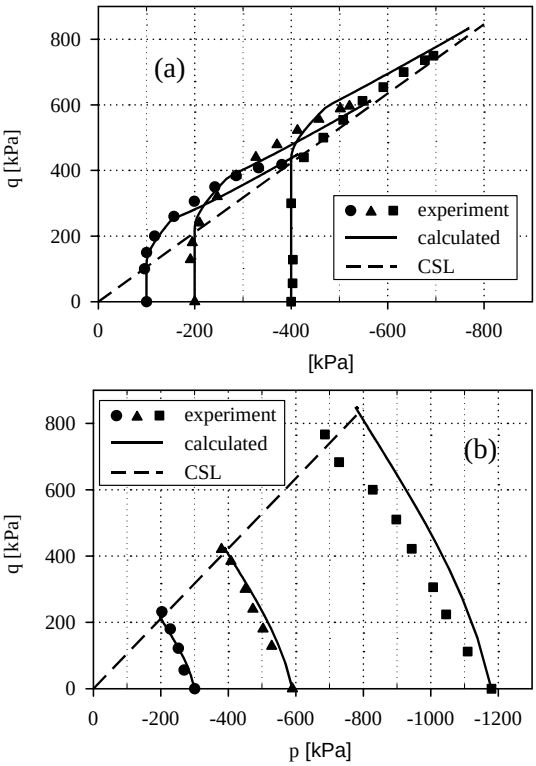

Figure 6: Undrained triaxial stress paths of overconsolidated (a) and normally consolidated (b) Vallericca clay

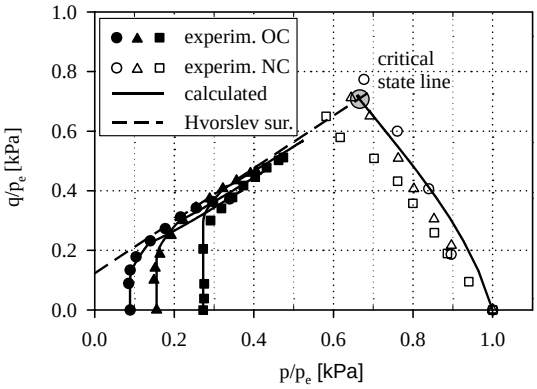

Figure 7: Normalized undrained stress paths

6 CONCLUSION

A novel approach to model deformation behavior and strength characteristics of highly overconsolidated, stiff clays has been presented. The model is based on the multilaminate framework and automatically takes into account anisotropy induced by plastic strains. Peak shear strength in the highly overconsolidated range is defined by a Hvorslev surface whose size depends on the degree of overconsolidation and the development of volumetric plastic strains. Dilatancy in the highly overconsolidated range is controlled by the distance between Hvorslev surface and critical state line, which is in good agreement with experimental data.

REFERENCES

[1] Bažant, Z.P. & Oh, B.H. 1986. Efficient Numerical Integration on the Surface of a Sphere, *Z. Angew. Math. Mech.* **66** (1) 37-49

[2] Burland, J.B., Rampello, S., Georgiannou, V.N. & Calabresi, G. 1996. A laboratory study of the strength of four stiff clays. *Geotechnique* **46** (3), 491-514.

[3] Callisto, L. & Rampello, S., 2004. An interpretation of structural degradation for three natural clays. *Can. Geotech. J.* **41** (6), 392-407.

[4] Price, A.M. & Farmer, I.W., 1981. The Hvorslev Surface in Rock Deformation. *Int. J. Rock Mech. Min. Sci. & Geomech. Abstr.* **18**, 229-234.

[5] Schweiger, H.F., Wiltafsky, C., Scharinger, F. & Galavi, V. 2009. A multilaminate framework for modelling induced and inherent anisotropy of soils. *Geotechnique* **59** (2), 87-101.